MODELING THE SOIL-TOOL-ROOT OR -STEM INTERACTION WITH COUPLED DISCRETE ELEMENT AND MASS-SPRING METHODS

László Pásthy and Kornél Tamás
Department of Machine and Product Design, Faculty of Mechanical Engineering, Budapest University of Technology and Economics, Műegyetem rkp. 3.,
H-1111 Budapest, Hungary
E-mail: pasthy.laszlo@edu.bme.hu, tamas.kornel@gt3.bme.hu

ABSTRACT

In the course of this research, a so-called mass-spring method was implemented in an in-house developed two-dimensional discrete element software, which enables the simulation of deformable, tear-able bodies, such as plant residues (stems or roots), or other agricultural fibrous materials. The operation of the numerical methods was illustrated with simulations where a rigid plate was moved horizontally against a plant residue modeled by the mass-spring method, pulled in an assembly of particles modeled by the discrete element method, and pulled in a combination of these. When evaluating the results, it was found that the improved numerical methods are able to work stable both separately and in interaction with each other, thus in the future it is possible to take plant residues as stems and roots into account during the simulations of the tillage process with their coupled application.

INTRODUCTION

The behaviour of granular materials can be effectively simulated with the discrete element method (DEM) (Cundall and Strack 1979), which has been used not only by researchers but also by engineers in the last decade. In the main steps of the method the reaction forces are calculated in the contacts between the rigid particles, and then the acceleration vector, velocity vector and the position of the partciles are calculated. Thus, processes based on the behaviour of particles such as tillage, mixing of granules and powders can be modeled with computer simulations. However, since during these simulations the solid bodies in contact with the particles are taken into account as rigid, the applicability of the method is limited by the magnitude of the force acting on the solid bodies. When these contact forces cause a significant deformation in the solid body, which already affects the movement of the particles, the discrete element method simulation alone is not sufficient, another calculation procedure is required to model the deformation of the solid body, which can run parallel with the discrete element method. Such simulations, which use several numerical methods, are called coupled simulations, the development of which is currently an intensively researched area.

A possible method for calculating the deformation of solid bodies is the so called mass-spring method, which models the solid body with mass points, springs and dampings. The method is primarily used to simulate the movement of two-dimensional surfaces. The LapSim software (Woodrum et al. 2006), for example, is a medical simulation program that models the movement of different tissues using the mass-spring method. The procedure is also used in software modelling clothing and textile (Gräff et al. 2004, Rony et al. 2007) and graphic-animation software (Derakhshani 2013). In addition to modeling two-dimensional surfaces, József Sebestyén extended the method to three-dimensional bodies in his master's thesis (Sebestyén 2018), thus the deformation of 3 dimensional objects can also be modeled with the developed procedure. The advantage of the method is that even real-time simulations are possible due to the low computational requirements. Another advantage of the mass-spring method is the easy understanding and application compared to other numerical methods.

One possible area of application of the mass-spring method can be the modeling of plant residues (stems or roots) left inside and on the surface of the soil as deformable bodies that can even tear. Although there was no reported example of the use of the mass-spring method for the modeling of stems or roots in the literature, the consideration of stems and roots in tillage simulations is increasingly of concern to researchers these days. In previous research, plant residues were mostly modelled with rigid spheres (Mao et al. 2020, Wang et al. 2020), multiple cylinders that are rigidly connected (Zeng et al. 2020), hinged spheres and cylinder elements (Guo et al. 2018) or deformable elements made up of rigid cylindrical elements (Bourrier et al. 2013, Tamás and Bernon 2021). These elements however were not capable of tearing or were able to tear only at the connection of the rigid cylinder elements. The mass-spring method, on the other hand, allows the deformation of all parts of the modeled body and the tear can occur in more places than in the case of the stem or root models used so far.

The aim of this research was to develop a coupled numerical method that enables the modeling of the interaction between granular materials and deformable bodies, as well as the modeling of the tear of deformable bodies using coupled discrete element method and mass-spring method. Furthermore an other aim was to to implement the procedure in a self-developed two-dimensional software, as well as to illustrate its functionality with soil tillage modeling simulations where a deformable plant residue, a rigid tool and a soil as a granular material are taken into account.

THEORETICAL BACKGROUND

The equations of the discrete element method were utilised based on our previous research (Pásthy et al. 2022). The contact forces between the particles, the deformable body and the rigid objects were calculated according to the Hertz-Mindlin contact model, which was also described in the mentioned publication.

The mass-spring method makes possible to model deformable bodies with mass points (nodes) placed in a specific grid and with parallely placed springs and dampings connecting the mass points according to given rules. Figure 1 shows the mass points in a two-dimensional grid and the different kind of springs and dampings connected to it.

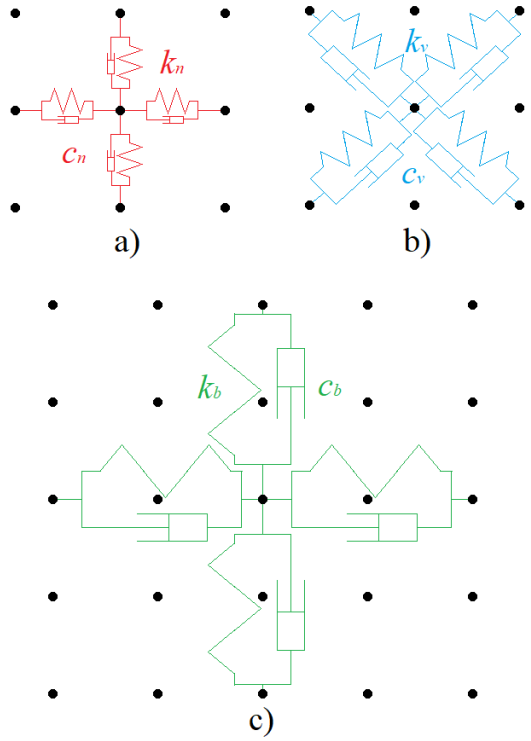

Figure 1: Springs and dampings connecting the mass points in a grid in a 2 dimensional case, a) structural springs (k_n [N m^{-1}]) and dampings (c_n [N s m^{-1}]), b) shear springs (k_v [N m^{-1}]) and dampings (c_v [N s m^{-1}]), c) flexural springs (k_b [N m^{-1}]) and dampings (c_b [N s m^{-1}])

Structural springs and dampings connect vertically and horizontally adjacent mass points (Figure 1 a). These elements return the grid nodes to a constant position relative to each other when the grid body is stretched or compressed. Shear springs and dampings connect oppositely adjacent mass points (Figure 1 b). These elements return the nodes to a constant position relative to each other when the grid is sheared. And the flexural springs connect the mass points that are two nodes apart vertically and horizontally (Figure 1 c). These elements return the nodes to a constant position relative to each other when the grid is bent.

The force arising in a spring is proportional to the relative displacement of the mass points and act in the direction of the straight line connecting the mass points between which the spring is placed. The force acting on the i-th node from a spring that connects the i-th and j-th node in the two-dimensional case is:

$$\boldsymbol{F_k} = -k \cdot \left[l - \sqrt{(x_i - x_j)^2 + (y_i - y_j)^2} \right] \cdot \begin{pmatrix} x_i - x_j \\ y_i - y_j \end{pmatrix} \cdot \frac{1}{\sqrt{(x_i - x_j)^2 + (y_i - y_j)^2}} \quad (1)$$

Where k [N m^{-1}] is the stiffness of the spring, l [m] is the initial distances between the i-th and j-th node, x_i, y_i [m] are the coordinates of the i-th node and x_j, y_j [m] are the coordinates of the j-th node.

The force arising in a damping is proportional to the relative velocity of the mass points and act in the direction of the straight line connecting the mass points, opposed to the relative velocity vector. The force acting on the i-th node from a damping that connects the i-th and j-th node in the two-dimensional case is:

$$\boldsymbol{F_c} = -c \cdot \begin{pmatrix} \dot{x}_i - \dot{x}_j \\ \dot{y}_i - \dot{y}_j \end{pmatrix} \quad (2)$$

Where c [N s m^{-1}] is the damping coefficient, $\dot{x}_i$ [m s^{-1}] is the x direction velocity component of the i-th node, $\dot{y}_i$ [m s^{-1}] is the y direction velocity component of the i-th node, $\dot{x}_j$ [m s^{-1}] is the x direction velocity component of the j-th node, $\dot{y}_j$ [m s^{-1}] is the y direction velocity component of the j-th node.

Equation of motion of a mass point:

$$\sum \boldsymbol{F_{kn}} + \sum \boldsymbol{F_{kv}} + \sum \boldsymbol{F_{kb}} + \sum \boldsymbol{F_{cn}} + \sum \boldsymbol{F_{cv}} + \sum \boldsymbol{F_{cb}} + \sum \boldsymbol{F_{outer}} = m \cdot \boldsymbol{a} \quad (3)$$

Where $\sum \boldsymbol{F_{kn}}$ [N] is the force resulting from the structural springs, $\sum \boldsymbol{F_{kv}}$ [N] is the force resulting from the shear springs, $\sum \boldsymbol{F_{kb}}$ [N] is the force resulting from the flexural springs, $\sum \boldsymbol{F_{cn}}$ [N] is the force resulting from the structural dampings, $\sum \boldsymbol{F_{cv}}$ [N] is the force resulting from the shear dampings, $\sum \boldsymbol{F_{cb}}$ [N] is the force resulting from the flexural dampings, $\sum \boldsymbol{F_{outer}}$ [N] is the vector sum of the outer forces, m is the mass of the mass point and $\boldsymbol{a}$ is the acceleration vector of the mass point.

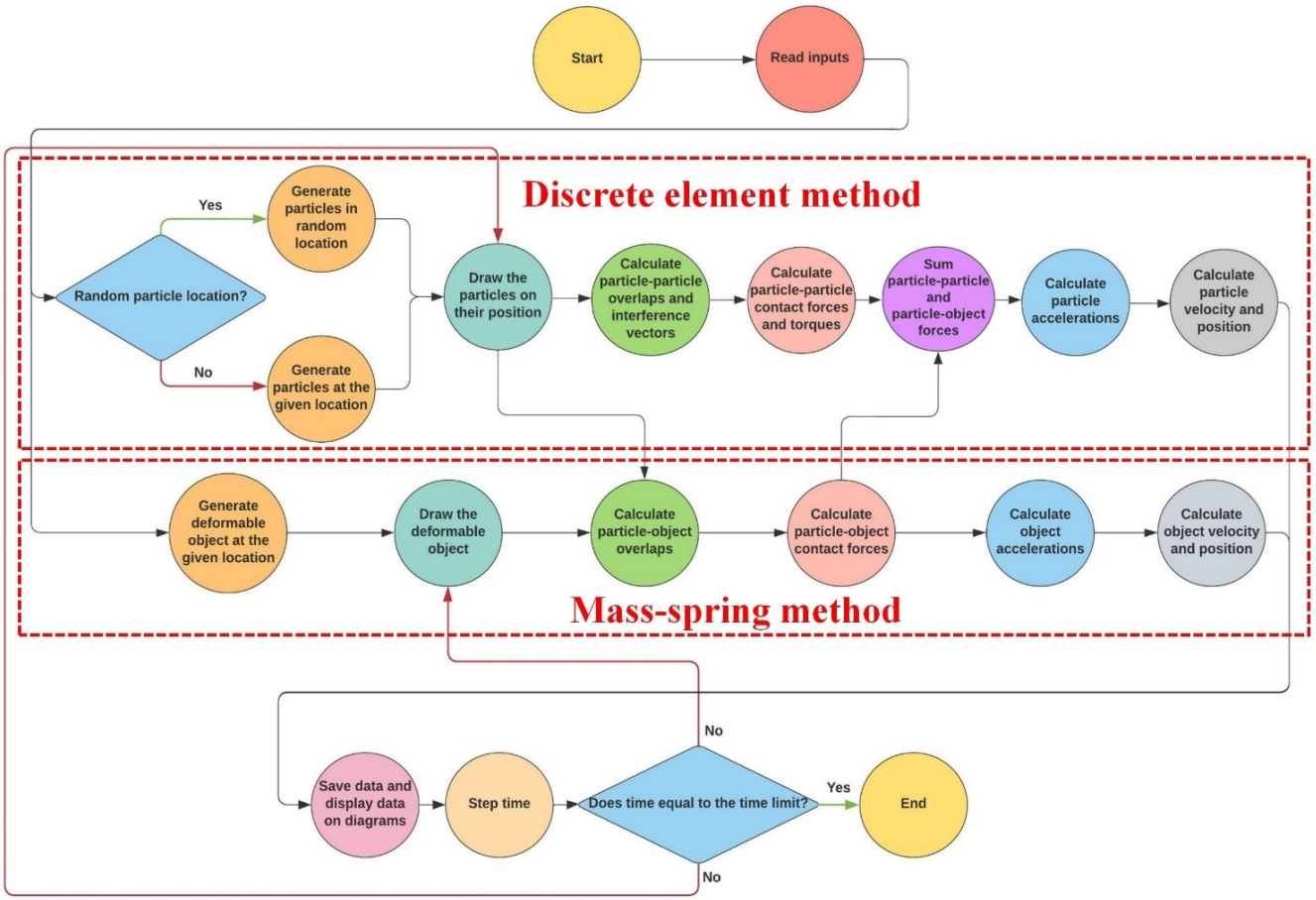

Figure 2: Simulation cycle of the coupled discrete-element and mass-spring methods

In the model, it is also possible to take the tearing into account. If the force between two nodes in the structural springs (structural strength), shear springs (shear strength) or flexural spring (flexral strength) exceeds a given value, the connection between the two nodes can be eliminated and deleted.

The simulation cycle is shown on Figure 2. The discrete element method that determines the movement of the particle assembly and the mass-spring method that calculates the deformation of the mass point grid is run in parallel. The steps of the discrete element calculation were applied according to our previous paper (Pásthy et al. 2022).

The first step of the mass-spring method is a graphical display, during which the connections (paralelly connected springs and dampings) between mass points are drawn in their current position as lines between the mass points. In addition to the position of connections and particles, it is also possible to display the force acting in the connections of the deformable body, the total force acting on the particles, and the von Mises equivalent stress state of the particles (Rojek et al. 2013), using a color scale.

The next step is to detect contacts, which is done in two substeps. First, the program finds the particles that are closer to a mass point than two times the particle radius. Next, in the case of a particle which fulfill the previous condition, 9 auxiliary points will be defined between the mass points, which border the grid and are closest to the examined particle. If there is a mass point or auxiliary point that is less distance away from the center of the particle than the particle radius, there is a contact between the particle and the deformable body. The overlap, which is proportional to the contact force by the Hertz-Mindlin contact model (Yang et al. 2020) is the difference between the particle radius and the distance between the center of the particle and the closest auxiliary or mass point. The contact force on the particle and on the deformable body is the same, but acts in the opposite direction. On the deformable body the force is proportionally distributed between the two mass points closest to the particle. The direction is parallel to the line that connects the center of the particle and the closest mass or auxiliary point (Figure 3).

After determining the contact forces of the particle-deformable body, the accelerations of the mass points are calculated based on Newton's laws. Following that, the velocity and position of the mass points are calculated. In the simulation behaviour of textiles (Gräff et al. 2004) the simultaneously applied predictor second-order Adams-Bashforth method (Adams and Bashforth 1883) and corrector second-order Adams-Moulton method (Moulton 1926) gave a surprisingly good result for the second-order system of nonlinear differential equations, so this method was used here as well.

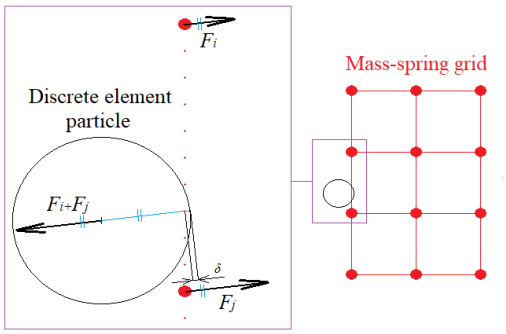

Figure 3. Contact of a particle and a deformable body represented by a mass-spring grid, (F_i is the force acting on the i-th node of the grid, F_j is the force acting on the j-th node of the grid and δ is the overlap between the particle and the grid).

Finally, the data is saved, and after that, the cycle starts from the beginning and the calculation is repeated until a specified time or until the STOP button is pressed.

The operation of the two simulation procedures was illustrated separately with two simulations, and then the coupling of the two procedures was presented in a third simulation. During all three simulations, a rigid flat plate moving in the horizontal direction was present, and the forces acting on it were plotted.

The simulations were run with the same parameters and the contact parameters were the same for all bodies (particles, boundary walls, rigid plate, deformable body), which are shown in Table 1. It should be noted that since our aim was only to implement the simulation procedures and demonstrate their functionality, the parameters were not calibrated, rather selected in order to maintain stability, but nevertheless they were suitable for validating the model.

Table 1: Simulation parameters (selected)

Name	Notation	Quantity	Unit
Discrete element parameters			
Particle density	ρ	1000	kg m $^{-3}$
Young's modulus	E	200000	Pa
Shear modulus	G	200000	Pa
Damping factor	β	20	-
Sliding friction coefficient	μ	0.5	-
Rolling friction coefficient	μ_0	0.5	-
Particle radius	R	0.01	m
Number of particles	N_p	230	-
Gravitational field (in vertical direction)	g	-9.81	m s^{-2}
Mass-spring paramteres			
Number of rows in the grid	N_r	10	-
Number of columns in the grid	N_c	3	-
Mass of a grid point	m	5	kg
Structural stiffness	k_n	10000	N m^{-1}
Shear stiffness	k_v	10000	N m^{-1}
Bending stiffness	k_b	10000	N m^{-1}
Structural damping	c_n	50	N s m^{-1}
Shear damping	c_v	50	N s m^{-1}
Bending damping	c_b	50	N s m^{-1}
Structural strength	F_{nmax}	40	N
Shear strength	F_{vmax}	40	N
Flexural strength	F_{vbmax}	40	N
General parameters			
Time step	Δt	0.0001	s
Working depth of rigid sheet	h	0.04	m
Speed of rigid sheet	v	0.1	m s^{-1}

RESULTS

In the first simulation, the operation of the mass-spring method was illustrated (Figure 4). A rigid flat plate was pulled horizontally against a deformable and tear-able body (grid body) made of 3 columns and 10 rows, where the grid points on the lower two levels were fixed. The rigid sheet can be considered as a model of a tillage tool, and the deformable body as a stem or root model.

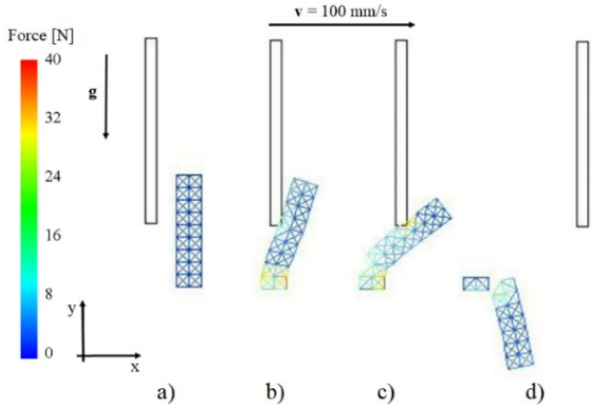

Figure 4: First simulation. Displacement of the rigid plate: a) 0 mm, b) 33 mm, c) 54 mm, d) 116 mm (the direction of the gravitational field **g** and the velocity vector of the rigid plate is represented by arrows, and the forces acting in the connections of the grid body is shown by a color scale).

It can be seen, that when the rigid plate hits the grid body it first bends (Figure 4 b), then with further movement of the rigid plate, the lower left vertical connection between a fixed grid point and an other grid point is torn, since the maximum force rises in that part of the grid body due to the bending (Figure 4 c). Finally, all the bonds connected to the lower, fixed nodes are torn and deleted, so the grid body is split into two parts (Figure 4 d). Without deleting the conncetions, the stability of the simulation was not adequate similarly to a previous publication (Tamás and Bernom 2021).

We plotted the change of the horizontal (x) and vertical (y) forces acting on the rigid plate, as well as their vector sum, which is shown on Figure 5.

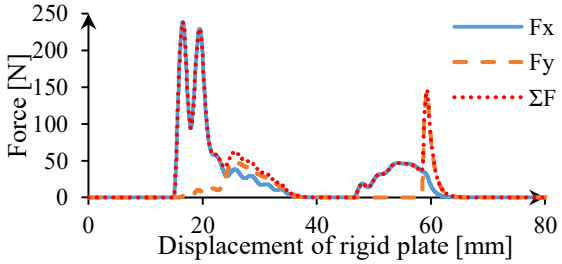

Figure 5: Force components acting on the rigid plate in the first simulation, (F_x is the horizontal force, F_y is the vertical force and ΣF is the vector sum of the two components).

It can be seen that when the rigid plate collides with the grid body, initially a horizontal force of 238 N occurs between the two bodies. After that, the horizontal force starts to decrease, and the vertical force increases, which is due to the fact that the bottom of the flat plate is more and more in contact with the grid body.

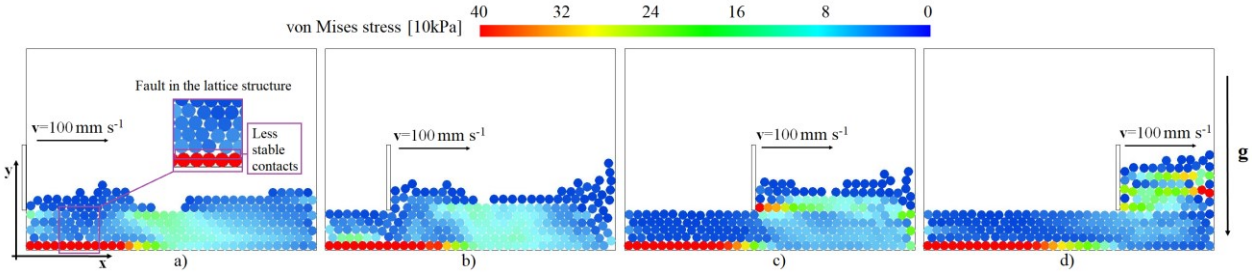

Figure 6: Second simulation. Displacement of the rigid sheet: a) 0 mm, b) 150 mm, c) 300 mm, d) 450 mm (the direction of the gravitational field **g** and the velocity vector of the rigid sheet is represented by arrows, and the von Mises equivalent stress state of the particles is shown by a color scale).

When the rigid plate moves 40 mm, it pushes the grid body away from itself, so the forces are temporarily eliminated. The two bodies come into contact again when the rigid plate moves 47 mm.

First, the right side of the rigid plate contacts the grid body, so the horizontal force increases to 50 N, and finally the bottom of the rigid plate contacts the grid body, so the vertical force increases to 150 N. Then the grid body splits into two parts and the upper part of the grid body falls down, so it is not contacting the rigid body anymore.

In the second simulation, the operation of the discrete element method was illustrated (Figure 6). A rigid plate was moved horizontally in a settled assembly consisting of 230 particles of the same diameter. The assembly of particles can be considered a model of a soil and the rigid plate a model of a tillage tool.

It can be seen that the software handles the contact between the flat plate and the discrete element particles stably. However a high stress state of the particles can be observed at the bottom left corner, which effect presumably is caused by the fact that in the course of the gravitational deposition the particles in the left corner could not form a perfect lattice structure, so at the bottom the particles have become in contact with each other in an energetically less stable position (Figure 6 a). In front of the rigid plate, the particles gradually pile up, and behind it, a flat layer forms at the depth where the rigid plate does not reach. It can also be observed that as soon as the flat plate pushes the particles against the right wall, the equivalent stress state of them increases (Figure 6 d).

The change of the horizontal (x) and vertical (y) forces acting on the rigid plate, as well as their vector sum was plotted, which is shown on Figure 7.

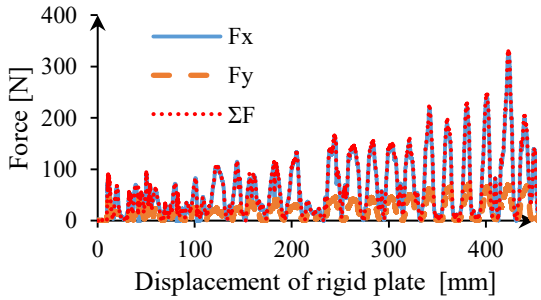

Figure 7: Force components acting on the rigid plate in the second simulation, (F_x is the horizontal force, F_y is the vertical force and ΣF is the vector sum of the two comonents).

The force acting on the rigid plate changes quasi-periodically. Suddenly the force reaches a local maximum, then decreases to zero, and this repeats. This is due to the discrete nature of the model. The particles in contact with the rigid plate are affected by such a force that they move away from the rigid plate, so the force decreases. Then, when the flat plate catches up with the particles, for a short period of time they come into contact again, and this repeats during the simulation. This phenomenon can be reduced by decreasing the particle size and setting appropriate material parameters and damping (e.g. viscous damping) (Horvath et al., 2022).

As more and more particles pile up in front of the flat plate, the local maximum of the force also takes on an increasing value. At the beginning, the local maximum values are below 100 N, and at the end of the simulation, the maximum force value is 341 N. This increase shows an exponential trend. The horizontal and vertical force components change proportionally, of which the horizontal force is three times larger.

In the third simulation the coupling of the mass-spring method and the discrete element method (Figure 8) was illustrated. A deformable, tear-able body consisting of 3 columns and 10 rows was inserted into an assembly of 230 particles, and a rigid flat plate was moved horizontally in the assembly. Similar to the first simulation the movement of the grid points on the lower two levels of the grid body were fixed in this case too. The assembly of particles can be considered as a discrete element model of a soil, the deformable body as a stem or root model, and the rigid sheet as a model of a tillage tool.

It can be seen that as soon as the rigid plate starts to push the particles in front of it, the grid body is deformed due to the particles piling up in front of it, and the stress in the particles next to the grid body increases (Figure 8 b). When the rigid plate gets into contact with the grid body, it undergoes even larger deformation (Figure 8 c), as a result of which the joints tear vertically in the middle and the lattice body splits in two parts.

At the beginning of the simulation the high stress state of the bottom left particles can be observed in this simaultion as well (Figure 8 a). However later the particles are able to form an energetically more stable structre, so the stresses are reduced in the bottom left corner (Figure 8 b and c).

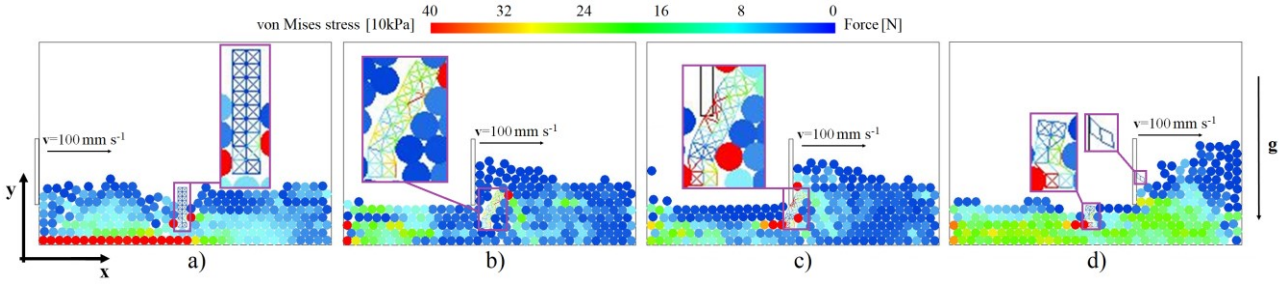

Figure 8: Third simulation. Displacement of the rigid sheet: a) 0 mm, b) 150 mm, c) 300 mm, d) 333 mm, e) 357 mm, f) 426 mm (the direction of the gravitational field **g** and the velocity vector of the rigid sheet is represented by arrows, the von Mises equivalent stress state of the particles and the forces acting in the connections of the grid body is shown by a color scale)

In the rest of the simulation, the lower part of the grid body bends down and remains in its original position, while the upper part is pushed in front of the rigid plate along with other particles (Figure 8 d).

The change of the horizontal (x) and vertical (y) forces acting on the rigid plate, as well as their vector sum was plotted, which is shown on Figure 9.

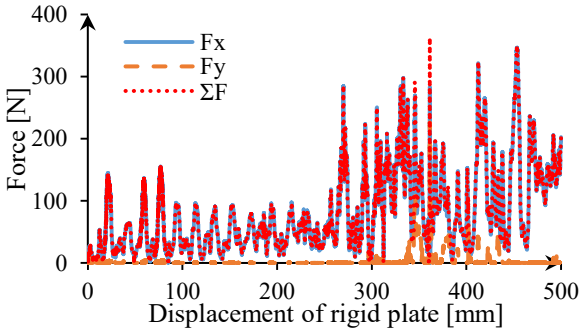

Figure 9: Force components acting on the rigid plate in the third simulation, (F_x is the horizontal force, F_y is the vertical force and ΣF is the vector sum of the two components).

The force acting on the rigid plate changes periodically similar to the second simulation, but here the increase of the local maximum does not show an exponential trend, and the vertical force component is negligible compared to the horizontal one until the contact of the rigid plate and the grid body. The local force maximum in the beginning of the simulation takes on a value of approximately 150 N, then at a displacement of 90 mm of the rigid plate, when the particles roll into the gaps in front of the grid body, the value of the local maximum decreases to 100 N. After the rigid plate moves 250 mm, the force begins to increase again due to the particles piling up in front of the grid body.

The local maximum values then reach and exceed 300 N. At a displacement of 357 mm, the rigid plate contacts the grid body, and since the nodes of the grid body are also in contact with the bottom of the rigid plate, a vertical force component appears. The force reaches its maximum value of 363 N just before the grid body is torn into two parts. After that, the force fluctuates between 20 N and 350 N until the end of the simulation.

Considering the results the interaction of the rigid plate, the particle assmebly and the grid body does not cause instability in the simulation, so that the coupled use of the mass-spring method and the discrete element method can be an effective tool for modelling plant residues (stems or roots) in the soil. However, this requires the extension of the two dimensional method to 3 dimensions, the use of multiple particle sizes and calibration tests to determine the appropriate simulation parameters.

CONCLUSION

The main novelty value of this research is the improvement of a coupling of the discrete element method with the so-called mass-spring method and implement it in an in-house developed 2 dimensional software to make possible the simulation of stems and roots in the soil-tool simulations.

The essence of the mass-spring method is to model the bodies with mass points and springs and dampings placed between them, which are deleted when specific force values are exceeded, allowing the simulation of deformable, tear-able bodies. The operation of the calculation methods was illustrated with simulations where a rigid flat plate was pulled horizontally against a grid body modeled with the mass-spring method, pulled in a particle assembly modeled with the discrete element method and pulled in a combination of them. When evaluating the results, it was found that the calculation procedures are able to operate stable both separately and in interaction with each other, thus in the future it is possible to take stem and root residues into account in soil tillage simulations with their coupled application. The force components acting on the rigid plate was plotted and it was found that the value of the forces varies periodically due to the discrete nature of the simulation. The largest force occurred in the last simulation (363 N), when the coupled interaction of the rigid plate, the particle assembly and the grid body was investigated.

The effect of the moving speed of the rigid plate on the simulation results could be a subjet of a further study. In addition a possible development could be the extension of the two methods into three dimensions, the implementation of particles of different sizes and/or of different shape in different size distributions in the simulations, as well as the calibration of the simulation parameters with laboratory tests. Furthermore in the future the mass-spring method may also provide an opportunity to simulate deformable tillage tools.

ACKONWLEDGEMENT

This paper was supported by the János Bolyai Research Scholarship of the Hungarian Academy of Sciences.

"Project no. TKP-6-6/PALY-2021 has been implemented with the support provided by the Ministry of Culture and Innovation of Hungary from the National Research, Development and Innovation Fund, financed under the TKP2021-NVA funding scheme.

REFERENCES

Bashforth, F. and J. C. Adams 1883. "An Attempt to test the Theories of Capillary Action by comparing the theoretical and measured forms of drops of fluid. With an explanation of the method of integration employed in constructing the tables which give the theoretical forms of such drops" *Cambridge*.

Bourrier, F., Kneib, F., Chareyre, B., & Fourcaud, T. 2013. "Discrete modeling of granular soils reinforcement by plant roots." *Ecological Engineering*, *61*, 646–657.

Cundall, P. A., & Strack, O. D. L. 1979. "A discrete numerical model for granular assemblies." *Géotechnique*. https://doi.org/10.1680/geot.1979.29.1.47

Derakhshani, D. 2012. "Introducing Autodesk Maya *2013*." *John Wiley & Sons*.

Goldenthal, R., Harmon, D., Fattal, R., Bercovier, M., & Grinspun, E. 2007. "Efficient simulation of inextensible cloth." In *ACM SIGGRAPH 2007 papers* 49.

Gräff, J. and J. Kuzmina. 2004. "Cloth simulation using mass and spring model". In *GÉPÉSZET 2004, Proceedings of the Fourth Conference on Mechanical Engineering*. Budapest, Magyarország: Budapest University of Technology and Economics 781 p. pp. 443-447. , 5 p.

Guo, Y., Wassgren, C., Curtis, J. S., & Xu, D. (2018). "A bonded sphero-cylinder model for the discrete element simulation of elasto-plastic fibers." *Chemical Engineering Science*, *175*, 118–129.

Horvath, D., Tamas, K., & Poos, T. (2022). Viscoelastic contact model development for the discrete element simulations of mixing process in agitated drum. *Powder Technology*, *397*, 117038.

Mao, H., Wang, Q., & Li, Q. 2020. "Modelling and simulation of the straw-grain separation process based on a discrete element model with flexible hollow cylindrical bonds." *Computers and Electronics in Agriculture*, *170*, 105229.

Moulton, F. R. 1926. "New methods in exterior ballistics" *University of Chicago Press.*

Pásthy, L., Gräff, J., & Tamás, K. 2022. "Development of a 2D discrete element software with LabView for contact model improvement and educational purposes" *In ECMS 2022. Proceedings of the 36th ECMS International Conference on Modelling and Simulation* (June), 203-209.

Rojek, J., Karlis, G. F., Malinowski, L. J., & Beer, G. 2013. "Setting up virgin stress conditions in discrete element models." *Computers and Geotechnics*, *48*, 228–248.

Sebestyén, J. 2018. "Rugalmas test anyagmodell szimulációja*"* [Diplomamunka].

Tamas, K., & Bernon, L. 2021. "Role of particle shape and plant roots in the discrete element model of soil–sweep interaction." *Biosystems Engineering*, *211*, 77–96.

Wang, Q., Mao, H., & Li, Q. 2020. "Modelling and simulation of the grain threshing process based on the discrete element method." *Computers and Electronics in Agriculture*, *178*, 105790.

Woodrum, D. T., Andreatta, P. B., Yellamanchilli, R. K., Feryus, L., Gauger, P. G., & Minter, R. M. 2006. "Construct validity of the LapSim laparoscopic surgical simulator." *The American Journal of Surgery*, *191*(1), 28–32.

Yang, W., Wang, M., Zhou, Z., Li, L., Yang, G., & Ding, R. 2020. "Research on the relationship between macroscopic and mesoscopic mechanical parameters of limestone based on Hertz Mindlin with bonding model." *Geomechanics and Geophysics for Geo-Energy and Geo-Resources*, *6*(4), 1–15.

Zeng, Z., & Chen, Y. 2019. "Simulation of straw movement by discrete element modelling of straw-sweep-soil interaction." *Biosystems Engineering*, *180*, 25–35.

AUTHOR BIBLIOGRAPHIES

LÁSZLÓ PÁSTHY is a PhD student at the Budapest University of Technology and Economics, Hungary where he received his MSc degree. His research field is coupled discrete element method (DEM) simulations. His e-mail address is: pasthy.laszlo@edu.bme.hu and his web-page can be found at https://gt3.bme.hu/oktatoi_oldal.php?lepes=4&oid=190.

KORNÉL TAMÁS is an associate professor at Budapest University of Technology and Economics where he received his MSc degree and then completed his PhD degree. His professional field is the modelling of granular materials with the use of discrete element method (DEM). His e-mail address is: tamas.kornel@gt3.bme.hu and his web-page can be found at https://gt3.bme.hu/oktatoi_oldal.php?lepes=4&oid=162.